ORIGINAL PAPER

Open Access

Nonlinear pre and post-buckled analysis of curved beams using differential quadrature element method

M. Zare[1] and A. Asnafi[2*]

Abstract

This paper studied the in-plane elastic stability including pre and post-buckling analysis of curved beams considering the effects of shear deformations, rotary inertia, and the geometric nonlinearity due to large deformations. Firstly, the governing nonlinear equations of motion were derived. The problem was solved performing both the static and dynamic analysis using the numerical method of differential quadrature element method (DQEM) which is a new and efficient numerical method for rapidly solving linear and nonlinear differential equations. Firstly, the method was applied to the equilibrium equations, leading to a nonlinear algebraic system of equations that would be solved utilizing an arc length strategy. Secondly, the results of the static part were employed to linearize the dynamic differential equations of motion and their corresponding boundary and continuity conditions. Without any loss of generality, a clamped-clamped curved beam under a concentrated load was considered to obtain the buckling loads, natural frequencies, and mode shapes of the beam throughout the method. To validate the proposed method, the beam was modeled using a finite element simulation. A great agreement between the results was seen that showed the accuracy of the proposed method in predicting the pre and post-buckling behavior of the beam. The investigation also included an examination of the curvature parameter influencing the dynamic behavior of the problem. It was shown that the values of buckling loads were completely influenced by the curvature of the beam; also, due to the sharp change of longitudinal stiffness after bucking, the symmetric mode shapes changed more than it was expected.

Keywords: Differential quadrature element method (DQEM), Curved beam vibration, Post-buckling, Buckling load, Arc length method, Non-linear analysis

Introduction

Curved beams have been a noticeable element in different applications and industries. The techniques involved in designing and constructing them have developed into many structural forms, such as mechanical devices, building arches, and bridges. As a result, it is important to have a better understanding of the dynamic stability of the subject to external loadings for the purpose of preventing possible accidents.

Many researches have been done in the field of stability of beam structures. Hummer (Hummer, 2013) investigated the buckling and post-buckling of beams taking into account both the influence of axial compressibility

and shear deformation on the basis of Reissner's relations. Bradford et al. (Bradford, Uy, & Pai, 2002) studied the in-plane elastic stability of arches under a central concentrated load analytically. A systematic method for the post-buckling analysis showing the importance of nonlinear terms of curved beams was established by Fan et al. (Fan et al., 2017). Addessi et al. (Addessi, Lacarbonara, & Paolone, 2005) obtained the natural frequencies and mode shapes of beams around their curved pre-stressed post-buckling configurations.

An investigation of the nonlinear buckling behavior of circular arches was done by Jianbei et al. (Jianbei, Mario, & David, 2014) by using the trapezoid method with Richardson extrapolation enhancement. Pi et al. (Pi, Bradford, & Tin-Loi, 2007) investigated the analytical solutions for in-plane nonlinear elastic behavior and the stability of elastically supported shallow circular arches. Their model was subjected to

* Correspondence: asnafi@shirazu.ac.ir
[2]Hydro-Aeronautical Research Center, Shiraz University, Shiraz 71348-51154, Iran
Full list of author information is available at the end of the article

a radial load uniformly distributed around the arch axis. A geometrically nonlinear finite element model of a composite curved beam was presented by Fraternali et al. (Fraternali, Spadea, & Ascione, 2013). They considered moderately large rotations, shear strains, as well as small axial strains.

Torabi et al. (Torabi, Afshari, & Aboutalebi, 2014) studied the free vibration of a Timoshenko beam with multiple cracks using DQEM. In order to check the accuracy of the proposed method, a comparison between obtained natural frequencies and those calculated by some other authors was done. In addition, they revealed that crack parameters influenced natural frequencies. Huynh et al. (Huynh, Luu, & Lee, 2017) studied the bending, buckling, and free vibration of curved beams, having variable curvature along the beam length by applying iso-geometric analysis. In their research, in addition to the impact of varying curvature, the effects of material distribution, aspect ratio, and slenderness ratio on the behavior of beams considering different boundary conditions were studied. Natural frequencies and buckling loads of a simply supported shallow circular arch subjected to initial axial force were investigated by Matsunaga (Matsunaga, 1995). In his research, the method of power series expansion of displacement components was applied to derive the equations. Liu et al. (Liu, Lu, Fu, et al., 2017) studied the out-of-plane dynamic instability of elastic shallow circular arches under an in-plane central concentrated periodic load. They derived the equations applying the Hamilton principle by considering the effects of geometric nonlinearity, additional concentrated weights, and damping. Pi et al. (Pi & Bradford, 2008) studied the dynamic in-plane buckling of a shallow pin-ended circular arch. In their study, a central radial load was considered to be exerted suddenly. They applied the method of conservation of energy as the criterion for dynamic buckling and analytical solutions of dynamic buckling loads. The first well-known governing vibration equations of preloaded, shear-deformable circular arches were derived by Huang et al. (Huang, Nieh, & Yang, 2003). They solved the governing equations using a static, closed-form solution, and an analytical dynamic series solution and dynamic stiffness matrices. Kounadis et al. (Kounadis, Gantes, & Bolotin, 1999) investigated the nonlinear dynamic buckling of structural systems qualitatively and quantitatively. In their study, multi-degree freedom structures which are sensitive to imperfection were investigated. A flexural-torsional buckling theory for circular arches was represented by Papangelis et al. (Papangelis & Trahair, 1986). In their method, the nonlinear expressions were derived and then substituted into the second variation of the total potential to obtain the buckling equation. In a study

done by Quan et al. (Quan, Cuong, & Duc, 2019), the nonlinear buckling and post-buckling of eccentrically oblique stiffened sandwich functionally graded double curved shallow shells resting on elastic foundations in the thermal environment was investigated. In their study, the shells were reinforced by functionally graded eccentrically oblique stiffeners with deviation angles. The stability of structures made of functionally graded material (FGM) has also been investigated in the literature (Anh, Bich, & Duc, 2015; Duc, 2014; Duc, Khoa, Nguyen, & Duc, 2019; Duc, Nguyen, & Khoa, 2017; Kim, Duc, Nam, & Van, 2019). In a study done by Duc (Minh & Duc, 2019), the effect of a central crack on the stability of a rectangular (FGM) plate was investigated. In that study, they applied the new third-order shear deformation plate theory (TSDT) and the finite element method (FEM) to obtain the results. Doan et al. (Doan, Van Do, Pham, & Duc, 2019) used the phase-field method to simulate the free vibration and buckling of cracked plates. They validated their results by numerically investigating free vibration and buckling of the aforementioned structure. There is a vast literature in domain discretization techniques and methods of continuous media; for example, see some other types in (Marin, Baleanu, & Vlase, 2017; Marin & Craciun, 2017; Marin & Nicaise, 2016).

In the previous studies, neglecting the rotary inertia effects, the buckling of non-shallow curved beams has been investigated. Moreover, in many studies, the approximated perturbation method has been used. In the present study, the pre- and post-buckling state of a generally curved beam with a radial concentrated force at the middle point of the beam is investigated. The problem is solved by performing both the static and dynamic analysis using the numerical method of the differential quadrature element method. In static analysis, the solution of the nonlinear equations is obtained applying the arc-length method. The buckling load is obtained considering the displacement of the middle point as a known parameter of the arc length method in the static analysis. Finally, the linearized dynamic differential equations of motion and their corresponding boundary and continuity conditions are transformed into an eigenvalue problem and the natural frequencies and mode shapes are evaluated.

Materials and methods
Governing equation of motion for a curved beam
The equation of motion for a curved beam's post-buckled state, taking into account the effects of shear deformation and rotary inertia, as well as, the extension of the neutral axis, can be written as (Jianbei et al., 2014):

$$N\left(\frac{1}{R} - \frac{\partial\phi}{\partial S}\right) - \frac{\partial Q}{\partial S} = -\gamma A \ddot{U} \tag{1}$$

$$Q\left(\frac{1}{R} - \frac{\partial\phi}{\partial S}\right) + \frac{\partial N}{\partial S} = \gamma A \ddot{W} \tag{2}$$

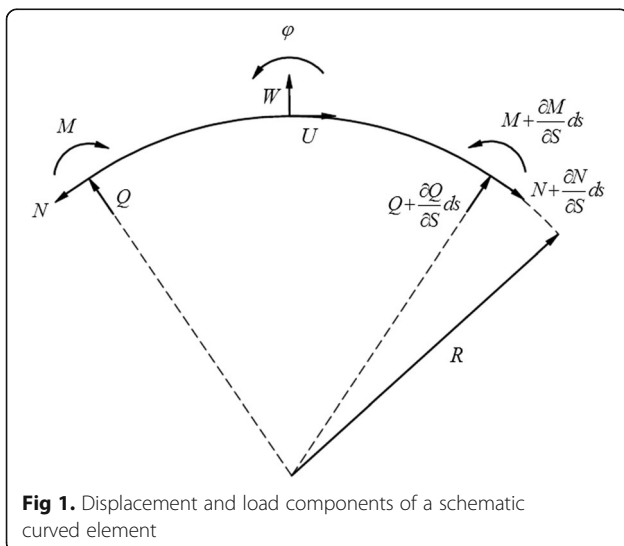$$\frac{\partial M}{\partial S} - N\frac{Q}{kAG} + Q\left(\frac{N}{EA} + 1\right) = \gamma A \ddot{\phi} \tag{3}$$

$$\frac{N}{EA} = \left(\left(\frac{\partial U}{\partial S} + \frac{W}{R} + 1\right)\cos(\phi) + \left(\frac{\partial W}{\partial S} - \frac{U}{R}\right)\sin(\phi) - 1\right) \tag{4}$$

$$\frac{Q}{kAG} = \left(-\left(\frac{\partial U}{\partial S} + \frac{W}{R} + 1\right)\sin(\phi) + \left(\frac{\partial W}{\partial S} - \frac{U}{R}\right)\cos(\phi)\right) \tag{5}$$

$$M = EI\frac{\partial\phi}{\partial S}, \tag{6}$$

where dot means the derivative with respect to time. As shown in Fig. 1, which represents an element of a curved beam, W, U, and ϕ denote the radial and tangential displacements, and the angle of rotation. Parameters M, N, and Q show the bending moment, normal and shear forces respectively. Moreover, A, I, γ, G, E, and k are the cross-section area of the beam, area moment of inertia of the cross-section, mass density per unit volume of the beam material, shear and Young's modulus of elasticity, and shear factor of the cross-section, respectively.

In what follows, the equations of motion are solved by the DQE method which is one of the efficient numerical methods for fast solving linear and nonlinear differential equations.

DQEM

The differential quadrature element method (DQEM) is a new and efficient numerical method for rapidly solving linear and nonlinear differential equations. The method is based on the differential quadrature (DQ) method which is an approximate method for expressing partial derivatives of a function at a point located in the domain of the function, as the weighted linear sum of the values of the variable function at all the defined precision points in the derivation direction. Equation (7) is the mathematical representation of the DQ expansion (Chen, 2005):

$$\left.\frac{df}{dx}\right|_{x=x_i} = \sum_{j=1}^{N} C_{ij}^{(1)} f_j, \quad i, j = 1, 2, 3, ..., N \tag{7}$$

where f is the desired function, N is the number of precision points, x_i is the precision associated with the ith point of the function domain and also represents the weighting coefficients used to find the first derivative of the function at the ith precision point of the function domain.

In our case study, the beam is discretized to m elements and each element itself is divided into N nodes (see Fig. 2). These nodes are the aforementioned precision points. In order to use Eq. (7), the physical coordinate θ is transformed to the natural coordinate x with such the following relation (Chen, 2005):

$$\theta = (1-x)\theta_1 + x\theta_N \tag{8}$$

Where θ_1 and θ_N are the angular coordinates of the first and Nth nodes of the element respectively. Note that x is a value in [0, 1] domain, i.e., ($0 < x < 1$). In fact, applying this relation, the differentiation with respect to angular coordinate θ can be obtained using Eq. (8). According to Eqs. (7) and (8), there are two important

Fig 1. Displacement and load components of a schematic curved element
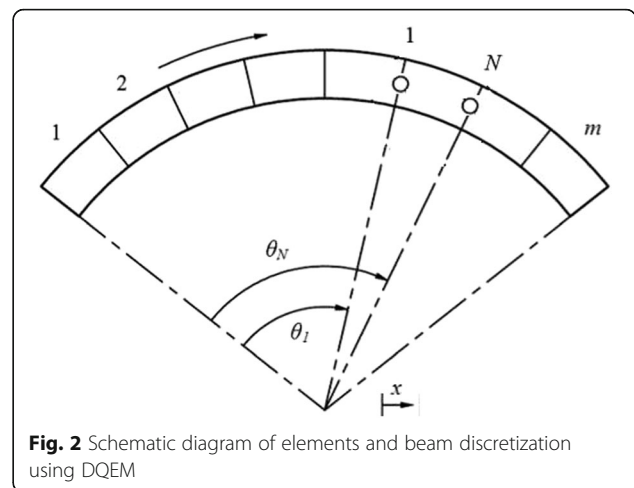
Fig. 2 Schematic diagram of elements and beam discretization using DQEM

factors in applying the DQ method; firstly, calculation of DQ weighting coefficients and, secondly, selection of the precision points. In this article, the Lagrangian functions were used to compute the weighted coefficients, and the Gauss–Lobatto Chebyshev polynomial was used to select the precision points. Finally, it is to be noted that to reach overall consistency, the continuity conditions at inter-element boundaries of two adjacent elements and the boundary conditions of the whole beam, as well as the governing equations on each element, must be satisfied.

As indicated previously, the beam is discretized to m elements and each element itself is divided into N nodes (see Fig. 2). Assuming a harmonic excitation of ω frequency for U, W, and ϕ in Eqs. (1–3), i.e., $\ddot{U} = -\omega^2 U$, $\ddot{W} = -\omega^2 W$, and $\ddot{\phi} = -\omega^2 \phi$, then applying the DQ discretization to the equations of motion at an interior node m^i of the element i, anybody can reach to such the following discrete equations (Jianbei et al., 2014):

$$N_{m^i}^i \left(\frac{1}{R} - \frac{\partial \phi_{m^i}^i}{\partial S} \right) - \frac{\partial Q_{m^i}^i}{\partial S} = \omega^2 \gamma^i A^i U_{m^i}^i, \tag{9}$$

$$Q_{m^i}^i \left(\frac{1}{R} - \frac{\partial \phi_{m^i}^i}{\partial S} \right) + \frac{\partial N_{m^i}^i}{\partial S} = -\omega^2 \gamma^i A^i W_{m^i}^i, \tag{10}$$

$$\frac{\partial M_{m^i}^i}{\partial S} - N_{m^i}^i \frac{Q_{m^i}^i}{KAG} + Q_{m^i}^i \left(\frac{N_{m^i}^i}{EA} + 1 \right) = -\omega^2 \gamma^i A^i \phi_{m^i}^i, \tag{11}$$

$$N_{m^i}^i = EA \left(\left(\frac{\partial U_{m^i}^i}{\partial S} + \frac{W_{m^i}^i}{R} + 1 \right) \cos(\phi_{m^i}^i) + \left(\frac{\partial W_{m^i}^i}{\partial S} - \frac{U_{m^i}^i}{R} \right) \sin(\phi_{m^i}^i) - 1 \right), \tag{12}$$

$$Q_{m^i}^i = kAG \left(-\left(\frac{\partial U_{m^i}^i}{\partial S} + \frac{W_{m^i}^i}{R} + 1 \right) \sin(\phi_{m^i}^i) + \left(\frac{\partial W_{m^i}^i}{\partial S} - \frac{U_{m^i}^i}{R} \right) \cos(\phi_{m^i}^i) \right), \tag{13}$$

$$M_{m^i}^i = EI^i \frac{\partial \phi_{m^i}^i}{\partial S}. \tag{14}$$

To solve the nonlinear vibration of the post-buckled curved beam (Eqs. (9–14)), first, the system of equations is solved statically to determine what the equilibrium shape is. As a result, considering small harmonic variations around the post-buckled equilibrium configuration, the solution can be written as the sum of the equilibrium and harmonic parts in the following form:

$$U_{m^i}^i = \left(U_{m^i}^i \right)_e + \left(U_{m^i}^i \right)_d \sin(\omega t), \tag{15}$$

$$W_{m^i}^i = \left(W_{m^i}^i \right)_e + \left(W_{m^i}^i \right)_d \sin(\omega t), \tag{16}$$

$$\phi_{m^i}^i = \left(\phi_{m^i}^i \right)_e + \left(\phi_{m^i}^i \right)_d \sin(\omega t), \tag{17}$$

$$N_{m^i}^i = \left(N_{m^i}^i \right)_e + \left(N_{m^i}^i \right)_d \sin(\omega t), \tag{18}$$

$$Q_{m^i}^i = \left(Q_{m^i}^i \right)_e + \left(Q_{m^i}^i \right)_d \sin(\omega t), \tag{19}$$

$$M_{m^i}^i = \left(M_{m^i}^i \right)_e + \left(M_{m^i}^i \right)_d \sin(\omega t). \tag{20}$$

Eliminating the time-dependent terms in Eqs. (9–11), the following equilibrium equations are obtained:

$$\left(N_{m^i}^i \right)_e \left(\frac{1}{R} - \frac{\partial \left(\phi_{m^i}^i \right)_e}{\partial S} \right) - \frac{\partial \left(Q_{m^i}^i \right)_e}{\partial S} = 0, \tag{21}$$

$$\left(Q_{m^i}^i \right)_e \left(\frac{1}{R} - \frac{\partial \left(\phi_{m^i}^i \right)_e}{\partial S} \right) + \frac{\partial \left(N_{m^i}^i \right)_e}{\partial S} = 0, \tag{22}$$

$$\frac{\partial \left(M_{m^i}^i \right)_e}{\partial S} - \left(N_{m^i}^i \right)_e \frac{\left(Q_{m^i}^i \right)_e}{KAG} + \left(Q_{m^i}^i \right)_e \left(\frac{\left(N_{m^i}^i \right)_e}{EA} + 1 \right) = 0, \tag{23}$$

$$\frac{\left(N_{m^i}^i \right)_e}{EA} - \left(\left(\frac{\partial \left(U_{m^i}^i \right)_e}{\partial S} + \frac{\left(W_{m^i}^i \right)_e}{R} + 1 \right) \cos\left(\left(\phi_{m^i}^i \right)_e \right) + \left(\frac{\partial \left(W_{m^i}^i \right)_e}{\partial S} - \frac{\left(U_{m^i}^i \right)_e}{R} \right) \sin\left(\left(\phi_{m^i}^i \right)_e \right) - 1 \right) = 0, \tag{24}$$

$$\frac{\left(Q_{m^i}^i \right)_e}{kAG} - \left(-\left(\frac{\partial \left(U_{m^i}^i \right)_e}{\partial S} + \frac{\left(W_{m^i}^i \right)_e}{R} + 1 \right) \sin\left(\left(\phi_{m^i}^i \right)_e \right) + \left(\frac{\partial \left(W_{m^i}^i \right)_e}{\partial S} - \frac{\left(U_{m^i}^i \right)_e}{R} \right) \cos\left(\left(\phi_{m^i}^i \right)_e \right) \right) = 0, \tag{25}$$

$$\left(M_{m^i}^i \right)_e - EI^i \frac{\partial \left(\phi_{m^i}^i \right)_e}{\partial S} = 0. \tag{26}$$

Now, small harmonic variations are considered around the post-buckled static equilibrium state. Substituting Eqs. (15–20) into (9–14), and removing the nonlinear terms, the linear dynamic equations of motion can be obtained as
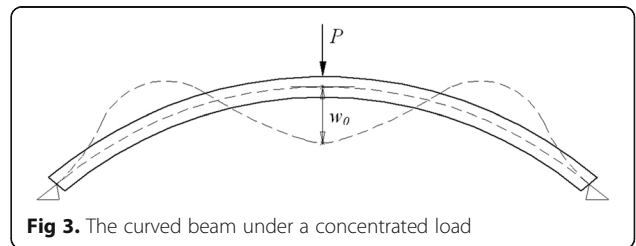
Fig. 3. The curved beam under a concentrated load
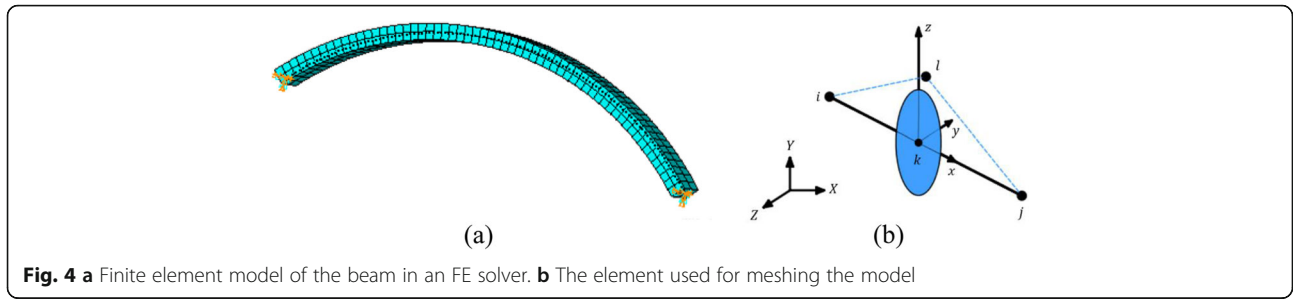
Fig. 4 a Finite element model of the beam in an FE solver. **b** The element used for meshing the model

$$\left(N^i_{m^i}\right)_e\left(-\frac{\partial(\phi^i_{m^i})_d}{\partial S}\right)$$
$$+\left(N^i_{m^i}\right)_d\left(\frac{1}{R}-\frac{\partial(\phi^i_{m^i})_e}{\partial S}\right)-\frac{\partial(Q^i_{m^i})_d}{\partial S}$$
$$= -\omega^2\gamma^i I^i\left(U^i_{m^i}\right)_d, \tag{27}$$

$$\left(Q^i_{m^i}\right)_e\left(-\frac{\partial(\phi^i_{m^i})_d}{\partial S}\right)$$
$$+\left(Q^i_{m^i}\right)_d\left(\frac{1}{R}-\frac{\partial(\phi^i_{m^i})_e}{\partial S}\right)+\frac{\partial(N^i_{m^i})_d}{\partial S}$$
$$= \omega^2\gamma^i I^i\left(W^i_{m^i}\right)_d, \tag{28}$$

$$\frac{\partial(M^i_{m^i})_d}{\partial S}+\left(Q^i_{m^i}\right)_d\left(N^i_{m^i}\right)_e\left(\frac{1}{EA}-\frac{1}{KAG}\right)+\left(N^i_{m^i}\right)_d\left(Q^i_{m^i}\right)_e\left(\frac{1}{EA}-\frac{1}{KAG}\right)+\left(Q^i_{m^i}\right)_d \tag{29}$$

$$\frac{\left(N^i_{m^i}\right)_d}{EA}-\left(\phi^i_{m^i}\right)_d\left(\frac{\left(Q^i_{m^i}\right)_e}{kAG}\right)-\left(\frac{\partial(W^i_{m^i})_d}{\partial S}-\frac{(U^i_{m^i})_d}{R}\right)\sin\left(\left(\phi^i_{m^i}\right)_e\right)$$
$$-\left(\frac{\partial(U^i_{m^i})_d}{\partial S}+\frac{(W^i_{m^i})_d}{R}\right)\cos\left(\left(\phi^i_{m^i}\right)_e\right)=0, \tag{30}$$

$$\frac{\left(Q^i_{m^i}\right)_d}{kAG}+\left(\phi^i_{m^i}\right)_d\left(\frac{\left(N^i_{m^i}\right)_e}{EA}+1\right)+\left(\frac{\partial(U^i_{m^i})_d}{\partial S}+\frac{(W^i_{m^i})_d}{R}\right)\sin\left(\left(\phi^i_{m^i}\right)_e\right)$$
$$-\left(\frac{\partial(W^i_{m^i})_d}{\partial S}-\frac{(U^i_{m^i})_d}{R}\right)\cos\left(\left(\phi^i_{m^i}\right)_e\right)=0, \tag{31}$$

$$\left(M^i_{m^i}\right)_d-EI^i\frac{\partial(\phi^i_{m^i})_d}{\partial S}=0. \tag{32}$$

Continuity conditions must also be applied at the interface of the beam segments. To have a better look at the equilibrium condition and the corresponding variation, the beam under a concentrated load (P), and its deformed centerline is shown in Fig. 3. In this figure, the solid arc is the initial shape of the beam and the dotted curve is the deformed shape of the centerline.

The radial and tangential displacements and the angular rotation continuity conditions at the inter-element boundaries of two adjacent elements i and $i + 1$, except for the peak of the beam, are expressed as

$$W^i_{N^i}=W^{i+1}_1,\ U^i_{N^i}=U^{i+1}_1,\ \phi^i_{N^i}=\phi^{i+1}_1 \tag{33}$$

Based on the action-reaction rule, to satisfy the continuity conditions at the inter-elements boundary of two adjacent elements, the normal and shear forces and the bending moment of the last node of segment i must be equal to corresponding loads of the first node of segment $i + 1$. In fact, with reference to Eqs. (12–14), the normal and shear forces and the bending moment continuity conditions at the inter-element boundary of two

Table 1 Mechanical properties of the curved beam

Property	Notation	Value
Radius of the beam axis	R	83 cm
Opening angle of the beam	θ	40°
Height of the cross-section	h	0.5 cm
Base of the cross-section	b	2 cm
Young's modulus	E	11 GPa
Poisson's ratio	v	0.3
Density	γ	7800 kg/m³
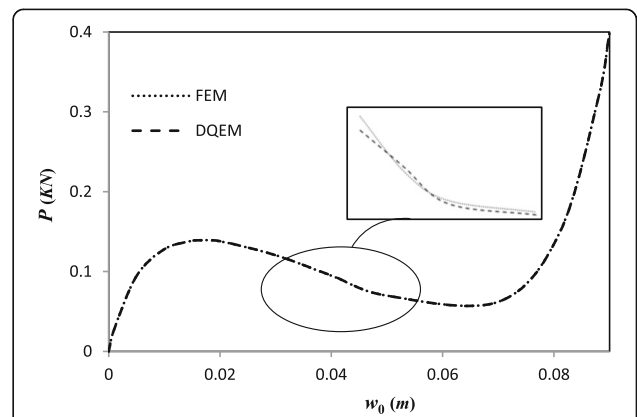
Fig. 5 The value of the concentrated buckling load versus the peak value of the radial displacement

Fig. 6 The value of the concentrated buckling load versus the peak value of the radial displacement for the beam at different curvatures. **a** 0.2, **b** 0.5, **c** 1.2, **d** 2.
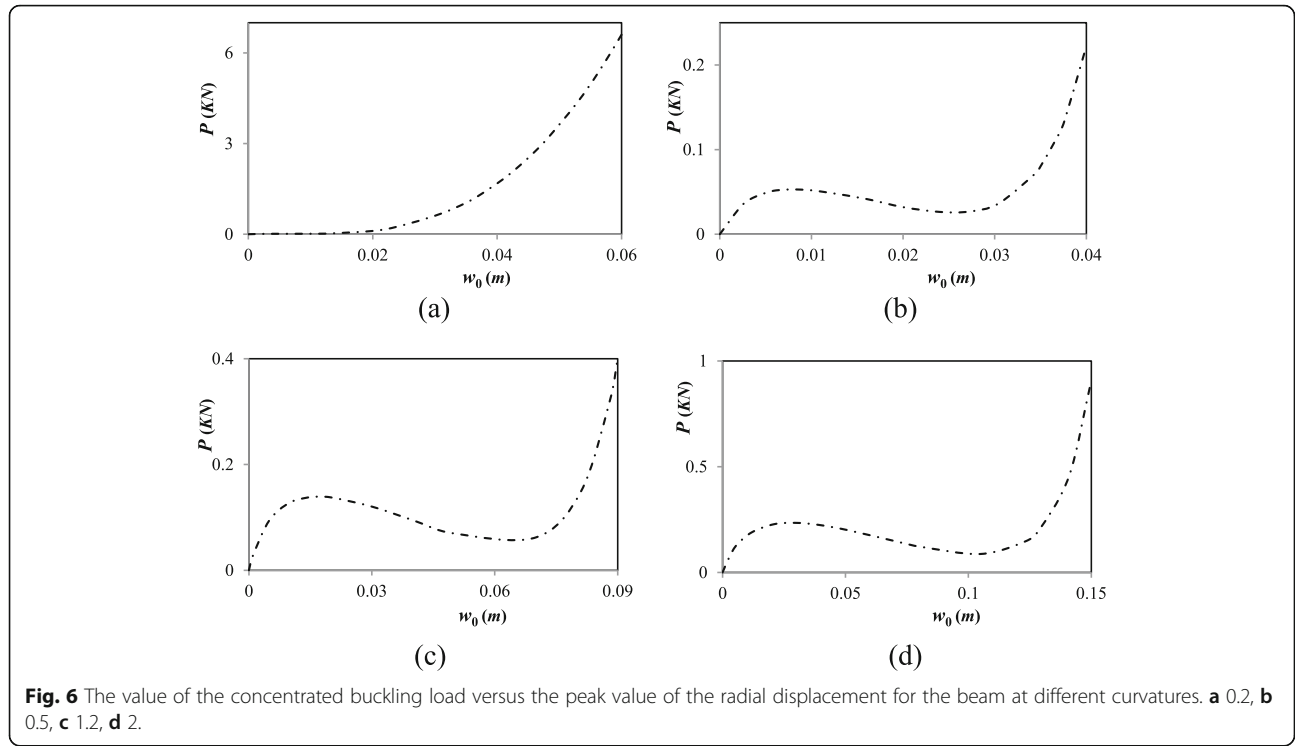
adjacent elements i and $i + 1$, can be expressed, respectively, as
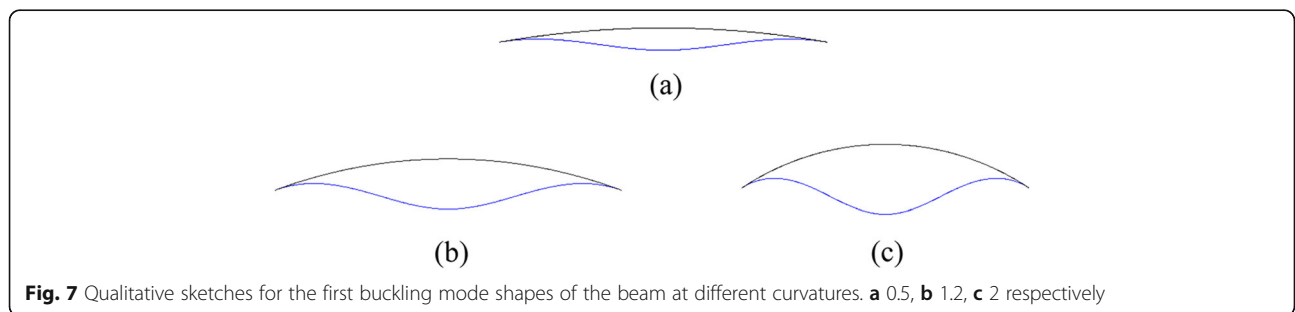
$$E^i A^i \left(\left(\frac{\partial u_{N^i}^i}{\partial S} + \frac{w_{N^i}^i}{R} + 1 \right) \cos\left(\phi_{N^i}^i\right) + \left(\frac{\partial w_{N^i}^i}{\partial S} - \frac{u_{N^i}^i}{R} \right) \sin\left(\phi_{N^i}^i\right) - 1 \right) =$$
$$E^{i+1} A^{i+1} \left(\left(\frac{\partial u_1^{i+1}}{\partial S} + \frac{w_1^{i+1}}{R} + 1 \right) \cos\left(\phi_1^{i+1}\right) + \left(\frac{\partial w_1^{i+1}}{\partial S} - \frac{u_1^{i+1}}{R} \right) \sin\left(\phi_1^{i+1}\right) - 1 \right),$$

$$(34)$$

$$k^i A^i G^i \left(-\left(\frac{\partial u_{N^i}^i}{\partial S} + \frac{w_{N^i}^i}{R} + 1 \right) \sin\left(\phi_{N^i}^i\right) + \left(\frac{\partial w_{N^i}^i}{\partial S} - \frac{u_{N^i}^i}{R} \right) \cos\left(\phi_{N^i}^i\right) \right) =$$
$$k^{i+1} A^{i+1} G^{i+1} \left(-\left(\frac{\partial u_1^{i+1}}{\partial S} + \frac{w_1^{i+1}}{R} + 1 \right) \sin\left(\phi_1^{i+1}\right) + \left(\frac{\partial w_1^{i+1}}{\partial S} - \frac{u_1^{i+1}}{R} \right) \cos\left(\phi_1^{i+1}\right) \right),$$

$$(35)$$

$$E^i I^i \frac{\partial \phi_{N^i}^i}{\partial S_{N^i}^i} = E^{i+1} I^{i+1} \frac{\partial \phi_1^{i+1}}{\partial S_1^i}. \tag{36}$$

The continuity conditions at the peak of the arch in the static state are

$$U_{N^i}^i = U_1^{i+1}, \phi_{N^i}^i = \phi_1^{i+1}, W_{N^i}^i = w_0, \ W_1^{i+1} = w_0$$
$$\frac{\partial u_{N^i}^i}{\partial S} = \frac{\partial u_1^{i+1}}{\partial S}, \ \frac{\partial \phi_{N^i}^i}{\partial S} = \frac{\partial \phi_1^{i+1}}{\partial S}, \ i = \frac{m}{2},$$

$$(37)$$

where w_0 is the radial displacement of the middle point of the beam (see Fig. 3).

Fig. 7 Qualitative sketches for the first buckling mode shapes of the beam at different curvatures. **a** 0.5, **b** 1.2, **c** 2 respectively

The continuity conditions at the peak for the dynamic state are similar to Eq. (37) except for w_0 which is considered to be 0.

To make the system of equations solvable, three boundary conditions must be considered at each end-point of the beam. Boundary conditions for a beam clamped at both ends in static and dynamic states are

$$W_1^1 = 0 \quad \phi_1^1 = 0 \quad U_1^1 = 0, \tag{38}$$

$$W_{N^i}^m = 0 \quad \phi_{N^i}^m = 0 \quad U_{N^i}^m = 0 . \tag{39}$$

Noting that for a perfect circular arch without any imperfection, the arch only deforms under a fully symmetric mode, so the beam is assumed to have some geometrical imperfections. In this study, the geometric imperfection functions are represented in terms of the first modal shape of the beam with an arbitrary amplitude of 0.001.

Applying the differential quadrature element method to the equations of motion of the beam, as well as, the continuity and boundary conditions, they are transformed into an algebraic system of eigenvalue problem that must be solved in terms of natural frequencies and mode shapes.

Formula for the buckling load

Regarding Fig. 3, if the load P is increased to a point which makes the beam unstable (the buckling load), the beam as a part of a detailed structure undergoes a large displacement with a small excitation. Since this phenomenon can fail the whole structure, predicting this force is an important part of a design in this respect. To model the application of buckling load, the radial displacement of the peak of the beam (w_0) is defined as the input of the arc length strategy meeting the converge criterion; so, the buckling load (P_c) is obtained as (Jianbei et al., 2014)

$$\begin{aligned} F_1 &= N_N^i \sin(\phi_N^i) + Q_N^i \cos(\phi_N^i), \\ F_2 &= N_1^{i+1} \sin(\phi_1^{i+1}) + Q_1^{i+1} \cos(\phi_1^{i+1}), \\ P_c &= \mid F_1 - F_2 \mid, \quad i = \frac{m}{2}. \end{aligned} \tag{40}$$

In the static analysis, this force can be equalized to the radial displacement in the continuity conditions at the peak of the arch as

$$\begin{aligned} &U_{N^i}^i = U_1^{i+1}, \phi_{N^i}^i = \phi_1^{i+1}, W_{N^i}^i = W_1^{i+1} \\ &\frac{\partial u_{N^i}^i}{\partial S} = \frac{\partial u_1^{i+1}}{\partial S}, \quad \frac{\partial \phi_{N^i}^i}{\partial S} = \frac{\partial \phi_1^{i+1}}{\partial S} \\ &F_1 = N_N^i \sin(\phi_N^i) + Q_N^i \cos(\phi_N^i), F_2 = N_1^{i+1} \sin(\phi_1^{i+1}) + Q_1^{i+1} \cos(\phi_1^{i+1}) \\ &P = \mid F_1 - F_2 \mid, \quad i = \frac{m}{2} \end{aligned} \tag{41}$$

Results and discussion

In this section, the results of our simulations in terms of the buckling load and the natural frequencies are obtained and interpreted.
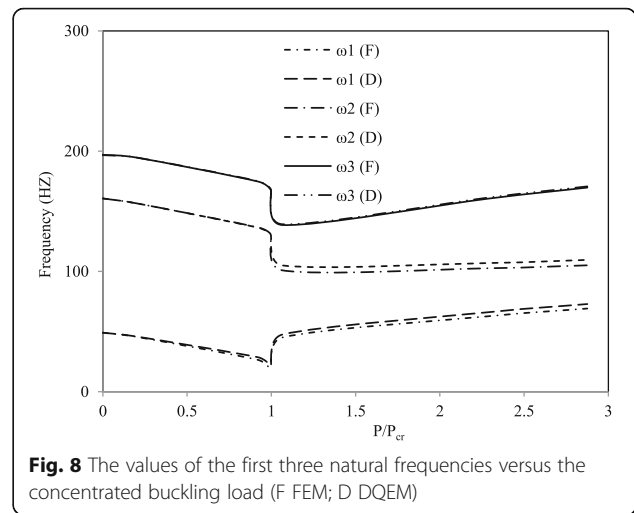

Fig. 8 The values of the first three natural frequencies versus the concentrated buckling load (F FEM; D DQEM)

### Validation of the method by a finite element simulation

In the aforementioned sections, the formulas of buckling load, as well as natural frequencies, have been derived using the proposed DQEM. With the purpose of validation of the accuracy of the proposed method, the beam is modeled in a finite element software (see Fig. 4), and the results obtained via DQE method are compared to those attained throughout the FE simulator. To analyze the nonlinear buckling behavior of the beam, the 3-node element BEAM189 was used in the FE simulation. In the analysis, 100 elements were used to have accurate results.

The buckling load

To ensure the validity and accuracy of the proposed methods, as an example, a clamped-clamped beam with
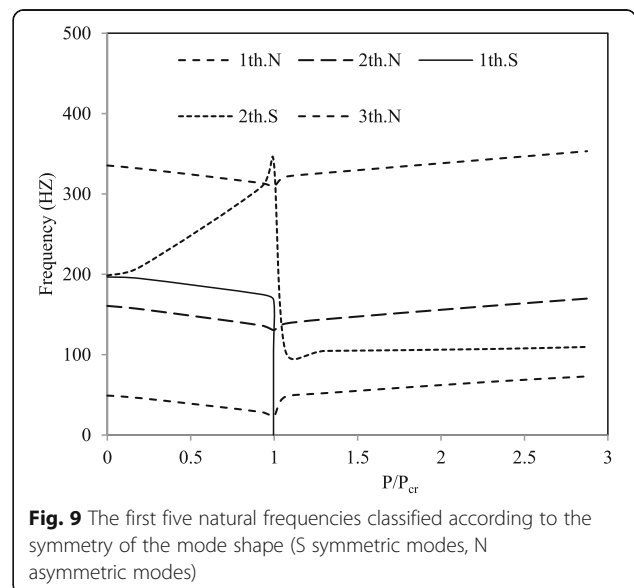
Fig. 9 The first five natural frequencies classified according to the symmetry of the mode shape (S symmetric modes, N asymmetric modes)

Fig. 10 The first five-mode shapes of the pre-buckled beam when **a** $P/P_c = 0.5$, **b** $P/P_c {}_r = 0.9$
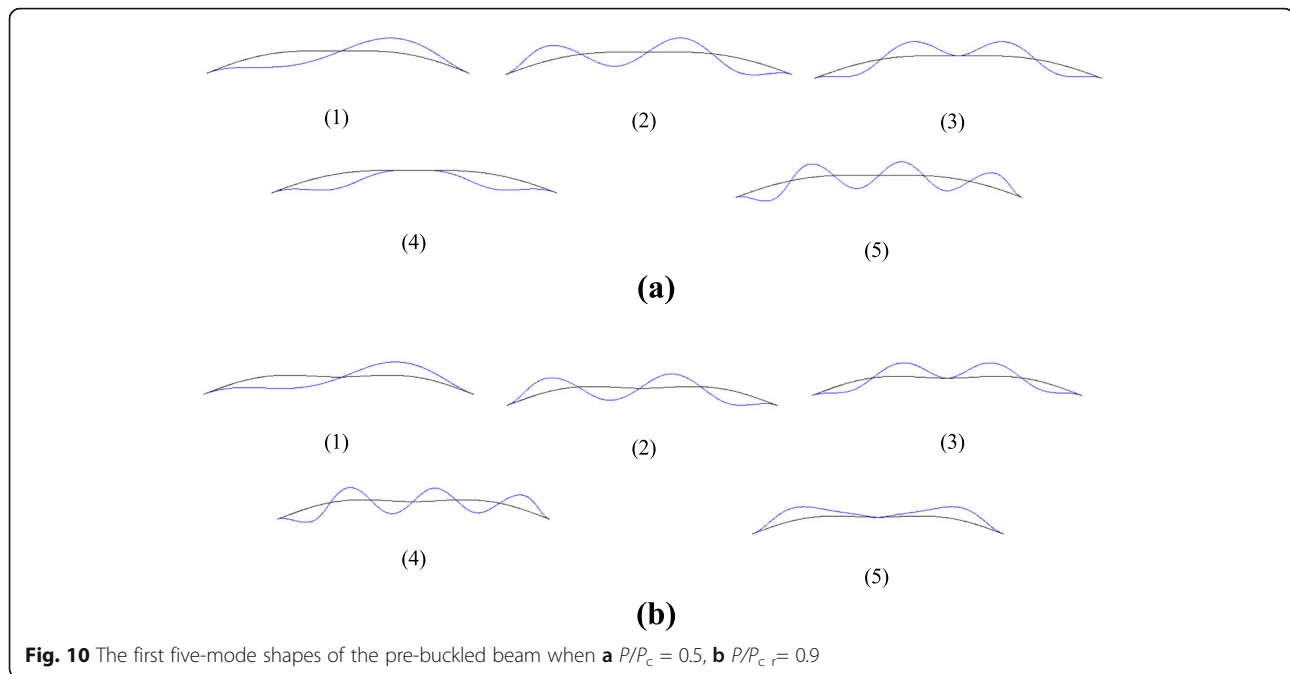
the properties listed in Table 1 and without any loss of generality is considered.

The magnitude of the concentrated load can be calculated using Eq. (40), which is plotted versus the radial displacement of the middle point (w_0) in Fig. 5. The results are also compared to ones obtained throughout a finite element simulator.

In this study, the results of the differential quadrature element method are obtained using a mesh composed of a series of four elements with 12 nodes in each element and adopting Gauss–Lobatto Chebyshev polynomials.

As shown in Fig. 5, the results of the current nonlinear analysis are in very good agreement with the corresponding finite element results which shows the high accuracy of the proposed method.

To investigate the effect of beam curvature on the buckling load, by assuming a constant value for the length of the beam specified in Table 1 and allowable changing in the opening angle of it, the value of

concentrated buckling load versus the radial displacement is drawn in Fig. 6.

Relative to Fig. 6, the curvature of the beam and the buckling load are proportional to each other which means a sufficient decrease in the curvature may prevent the buckling phenomenon. In addition, the beams with lower curvatures undergo buckling at a smaller peak value of the radial displacement. In other words, they show a lower deformation in the post-buckling state (see qualitative Fig. 7).

The natural frequencies

Solving the aforementioned eigenvalue problem, the natural frequencies can also be obtained. To show the accuracy of the results, a comparison between the DQEM natural frequencies and those obtained by the finite element method is done in Fig. 8 for the three lowest natural frequencies in the pre and post-buckling ranges.

Fig. 11 The first four mode shapes of the post-buckled beam when $P/P_{cr} = 2$
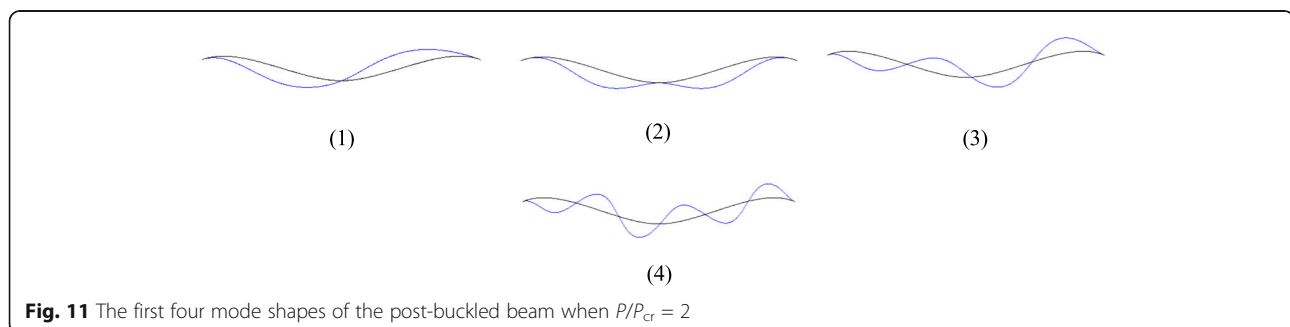
In this diagram, F and D show the FEM and DQEM results respectively.

In the above figure, it is worth noting that the agreement between the results obtained with the FE and DQE methods are very good up to the pre-buckling state; thereafter, a deviation is observed due to a little difference between the buckling loads obtained by these two methods. On the other hand, in the post-buckling state, the natural frequencies are more sensitive to the pre-stress effects, especially for the first and second natural frequencies.

In order to study the effect of buckling on the symmetry of the mode shapes, in Fig. 9, the first five natural frequencies are classified according to the symmetry of the corresponding mode shapes. In this diagram, the letters S and N denote the symmetric and asymmetric modes respectively.

As seen from the above figure, the first, the second and the third asymmetric modes are flexural modes, whereas the first and the second symmetric modes are longitudinal-flexural. The figure shows that as the applied concentrated load increases from zero to the buckling load, the first three asymmetric natural frequencies decrease smoothly due to the reduction in beam bending stiffness. Just after buckling occurs, a jump in the frequencies is seen that is due to a sudden increase of beam stiffness at this condition. After buckling, all the asymmetric frequencies increase with a much smaller rate owing to the increase in the bending stiffness caused by the change in the beam curvature.

Regarding Fig. 9, the behavior of the symmetric mode shapes is different. In the range under the critical buckling load, the natural frequencies of the first symmetric mode decreases smoothly due to the reduction in the total stiffness; however, the second symmetric natural frequency in which the longitudinal stiffness is dominant with respect to the flexural stiffness, increases rapidly up to the buckling value. In this range, it crosses the third asymmetric mode curve and therefore the mode transition phenomenon occurs (see also about this phenomenon in ref. (Tarnopolskaya & De Hoog, 1999)). In the post-buckling state, the dynamic longitudinal-induced stiffness suppresses the elastic flexural stiffness in both of the symmetric natural frequencies due to the large deformation of the beam; so, the second symmetric frequency shows a sharp decrease while the first one completely vanishes (Figs. 10 and 11).

In order to have a better understanding of the crossover of the frequency curves, in Figs. 10 and 11 the mode shapes corresponding to the pre-buckling state and those corresponding to the post-buckling state are shown, respectively:

Conclusion

In this study, the DQE and FE methods were implemented to investigate the behavior of a curved beam in the pre- and post-buckled state, taking into account the effects of shear deformation, rotary inertia, the extension of the neutral axis, the geometric nonlinearity due to the large deformation, and the beam imperfection.

The solution of the non-linear differential equations was performed including the static and dynamic parts. The differential quadrature element method along with an arc length strategy was used to solve the static part. Utilizing the results of this part, the DQEM was used to solve the linearized dynamic part. A clamped-clamped beam was considered under a concentrated load; however, the method could be used for other types of loadings and boundary conditions by changing the boundary conditions as well as the continuity conditions at the point of exerting load (Eqs. (37–39)). The effect of curvature on the buckling load was examined. In addition, increasing the concentrated load on the topology of the mode shapes and the values of the natural frequencies of the beam were studied. The results were validated by comparing to the corresponding same conditions FEM results. It was shown that for clamped–clamped beam, the asymmetric flexural frequencies decreased up to buckling and then increased smoothly after that point. However, the longitudinal-flexural symmetric frequencies showed a different behavior due to overcoming the longitudinal stiffness to the flexural one. Before buckling, the first natural frequency decreased smoothly while the second one experienced a sharp increase. After buckling, due to a severe drop in the longitudinal stiffness, the first symmetric frequency vanished, but the second one declined considerably.

Finally, it was concluded that firstly, the buckling phenomenon and the values of buckling loads were completely influenced by the curvature of the beam. Secondly, due to the sharp change of longitudinal stiffness after bucking, the symmetric mode shapes changed more than it was expected.

Authors' contributions

MZ surveyed the history of the research, derived, and solved the equations and drew the figures in corresponding software and wrote the first draft of the article. AA interpreted the results and wrote the final abstract and conclusion of the article. All authors read and approved the final manuscript.

Authors' information

M. Zare is an alumni of MSc. of mechanical engineering at the Shahid Chamran University of Ahvaz, Ahvaz, Iran. A. Asnafi is an associate professor of mechanical engineering at Shiraz University, Shiraz Iran.

Availability of data and materials

Data sharing not applicable to this article as no datasets were generated or analyzed during the current study.

Competing interests

The authors declare that they have no competing interests.

Author details

[1]Department of Mechanical Engineering, Shahid Chamran University, Ahvaz 61355, Iran. [2]Hydro-Aeronautical Research Center, Shiraz University, Shiraz 71348-51154, Iran.

References

Addessi, D., Lacarbonara, W., & Paolone, A. (2005). On the linear normal modes of planar pre-stressed. *Journal of Sound and Vibration, 284*, 1075–1097.

Anh, V. T. T., Bich, D. H., & Duc, N. D. (2015). Nonlinear stability analysis of thin FGM annular spherical shells on elastic foundations under external pressure and thermal loads. *European Journal of Mechanics - A/Solids, 50*, 28–38.

Bradford, M. A., Uy, B., & Pai, Y. L. (2002). In-plane elastic stability of arches under a central concentrated load. *Journal of Engineering Mechanics, 128*, 710–719.

Chen, C. N. (2005). DQEM analysis of in-plane vibration of curved beam structures. *Advances in Engineering Software, 36*, 412–424.

Doan, D. H., Van Do, T., Pham, P. M., & Duc, N. D. (2019). Validation simulation for free vibration and buckling of cracked Mindlin plates using phase-field method. *Mechanics of Advanced Materials and Structures, 26*, 1018–1027.

Duc, N. D. (2014). *Nonlinear static and dynamic stability of functionally graded plates and shells*. Hanoi: Vietnam National University Press.

Duc, N. D., Khoa, N. D., Nguyen, P. D., & Duc, N. D. (2019). An analytical solution for nonlinear dynamic response and vibration of FG-CNT reinforced nanocomposite elliptical cylindrical shells resting on elastic foundations. *ZAMM-Journal of Applied Mathematics and Mechanics*, 1–20.

Duc, N. D., Nguyen, P. D., & Khoa, N. D. (2017). Nonlinear dynamic analysis and vibration of eccentrically stiffened S-FGM elliptical cylindrical shells surrounded on elastic foundations in thermal environments. *Thin-Walled Structures, 117*, 178–189.

Fan, Z., Wu, J., Ma, Q., Liu, Y., Su, Y., & Hwang, K. C. (2017). Post-Buckling Analysis of Curved Beams foundations. *Journal of Applied Mechanics, 84*, 1–15.

Fraternali, F., Spadea, S., & Ascione, L. (2013). Buckling behavior of curved composite beams with different elastic response in tension and compression. *Composite Structures, 100*, 280–289.

Huang, C. S., Nieh, K. Y., & Yang, M. C. (2003). In-plane free vibration and stability of loaded and shear-deformable circular arches. *International Journal of Solids and Structures, 40*, 5865–5886.

Hummer, A. (2013). Exact solutions for the buckling and postbuckling of shear-deformable beams. *Acta Mechanica, 224*, 1493–1525.

Huynh, T. A., Luu, A. T., & Lee, J. (2017). Bending, buckling and free vibration analyses of functionally graded curved beams with variable curvatures using isogeometric approach. *Meccanica*, 1–20.

Jianbei, Z., Mario, M. A., & David, C. K. (2014). In-plane nonlinear buckling of circular arches including shear deformations. *Archive of Applied Mechanics, 84*, 1841–1860.

Kim, S. E., Duc, N. D., Nam, V. H., & Van, N. (2019). Nonlinear vibration and dynamic buckling of eccentrically oblique stiffened FGM plates resting on elastic foundations in thermal environment. *Thin-Walled Structures, 142*, 287–296.

Kounadis, A. N., Gantes, C. J., & Bolotin, V. V. (1999). Dynamic buckling loads of autonomous potential systems based on the geometry of the energy surface. *International Journal of Engineering Science, 37*, 1611–1628.

Liu, A., Lu, H., Fu, J., et al. (2017). Analytical and experimental studies on out-of-plane dynamic instability of shallow circular arch based on parametric resonance. *Nonlinear Dynamics, 87*, 87–677.

Marin, M., & Nicaise, S. (2016). Existence and stability results for thermoelastic dipolar bodies with double porosity. *Continuum Mechanics and Thermodynamics, 28*(6), 1645–1657.

Marin, M., Baleanu, D., & Vlase, S. (2017). Effect of microtemperatures for micropolar thermoelastic bodies. *Structural Engineering and Mechanics, 61*(3), 381–387.

Marin, M., & Craciun, E. M. (2017). Uniqueness results for a boundary value problem in dipolar thermoelasticity to model composite materials. *Composites Part B: Engineering, 126*, 27–37.

Matsunaga, H. (1995). In-plane vibration and stability of shallow circular arches subjected to axial forces. *International Journal of Solids and Structures, 13*, 469–482.

Minh, P. P., & Duc, N. D. (2019). The effect of cracks on the stability of the functionally graded plates with variable-thickness using HSDT and phase-field theory. *Composites Part B: Engineering, 175*, 1–9.

Papangelis, J. P., & Trahair, N. S. (1986). Flexural-torsional buckling of arches. *Journal of Structural Engineering, 112*, 889–906.

Pi, Y. L., & Bradford, M. A. (2008). Dynamic buckling of shallow pin-ended arches under a sudden central concentrated load. *Journal of Sound and Vibration, 317*, 898–917.

Pi, Y. L., Bradford, M. A., & Tin-Loi, F. (2007). Nonlinear analysis and buckling of elastically supported circular shallow arches. *International Journal of Solids and Structures, 44*, 2401–2425.

Quan, T. Q., Cuong, N. H., & Duc, N. D. (2019). Nonlinear buckling and post-buckling of eccentrically oblique stiffened sandwich functionally graded double curved shallow shells. *Aerospace Science and Technology, 90*, 169–180.

Tarnopolskaya, T., & De Hoog, F. R. (1999). Low-frequency mode transition in the free in-plane vibration of curved beams. *Journal of Sound and Vibration, 228*, 69–90.

Torabi, K., Afshari, H., & Aboutalebi, F. H. (2014). A DQEM for transverse vibration analysis of multiple cracked non-uniform Timoshenko beams with general boundary conditions. *Computers & Mathematics with Applications, 67*, 527–541.

Publisher's Note

Springer Nature remains neutral with regard to jurisdictional claims in published maps and institutional affiliations.